Journal of Molecular Liquids 222 (2016) 456–462

Contents lists available at ScienceDirect

Journal of Molecular Liquids

journal homepage: www.elsevier.com/locate/molliq

The adsorption of Eu(III) on carbonaceous nanofibers: batch experiments and modeling study

Zhongxiu Jin [a,b], Xia Liu [b], Shengxia Duan [b], Xinjun Yu [c], Yongshun Huang [b,c,*], Tasawar Hayat [d], Jiaxing Li [b,d]

[a] Central Laboratory of Preventive Medicine, Anhui Medical University, Hefei 230032, P.R. China
[b] Institute of Plasma Physics, Chinese Academy of Sciences, P.O. Box 1126, Hefei 230031, P.R. China
[c] University of Cincinnati, Cincinnati, OH, 45220, United States
[d] NAAM Research Group, Faculty of Science, King Abdulaziz University, Jeddah 21589, Saudi Arabia

ARTICLE INFO

Article history:
Received 20 June 2016
Accepted 17 July 2016
Available online 19 July 2016

Keywords:
Carbonaceous nanofiber
Adsorption
Eu(III)

ABSTRACT

Carbonaceous nanofibers (CNFs) were synthesized by a hydrothermal carbonization method and characterized by microstructure characterization methods (SEM, TEM, XPS, FTIR) and potentiometric titration. The effect of the environmental facts on the adsorption of Eu(III) on CNFs were examined by the batch experiments. The maximum adsorption capacity of Eu(III) on CNFs was calculated to be 62.6 $mg \cdot g^{-1}$ at pH 4.5 and 288 K. The thermodynamic parameters from Eu(III) adsorption isotherms at three temperatures suggested that this adsorption process was both spontaneous and endothermic. The CNFs/Eu(III) interactions were investigated by using diffuse layer modeling. The combination of a predominated $\equiv XOEu(OH)^{+}$ complex at pH < 3.5 and $\equiv XOEu(OH)^{+}$ and $\equiv SOEu(OH)_2$ complex at pH > 3.5 was consistent with the experiment data. CNFs can be regarded as a promising environmental functional nanomaterial for the removal of lanthanides from radionuclide contaminated water.

1. Introduction

Radioactive pollution in water is a serious environmental problem all over the world, therefore, the safe treatment of radionuclide contaminated water is very important to environmental treatment. Europium (Eu(III)) is a typical trivalent lanthanide with comparable physicochemical properties and similar environmental migration characters as other lanthanides [1]. The Eu(III) adsorption on alumina [2,3], TiO_2 [4,5], clay minerals [6,7], MWCNTs [8–10] and graphene oxide [11,12] have been widely investigated. However, most adsorbents presented low adsorption capacities, which significantly impede the Eu(III) removal from radionuclide contaminated water. Many high effective carbonaceous materials have been proposed as adsorbents to remove radionuclide Eu(III)from contaminated water recently.

Carbonaceous nanofibers (CNFs) produced from glucose hydrothermally have drawn extensive attentions recently. Its synthetic material (glucose) is environmental benign and easy to obtain from the nature [13]. The membrane made from CNFs are also regarded as suitable materials to remove organic dyes, metal ions (such as Pb(II) and Cr(VI)) via adsorption by electrostatics, complexation, or hydrogen-bonding [14]. The membrane of the CNFs has been used to remove heavy metal ions in water transmembrane treatment [15]. Zhang et al. [16] reported U(VI) adsorbed behavior on CNFs and the interactions between U(VI) and CNFs. However, few reports on the interactions and mechanism study between Eu(III) with CNFs has been researched. The removal of Eu(III) on the CNFs from contaminated water is necessary to be investigated.

In this paper, we will (1) fabricate CNFs and carry out their microscopic and macroscopic characterizations; (2) apply the as-prepared CNFs for Eu(III) concentration by considering the influencing factors; (3) reveal the adsorption mechanism with the aid of complexation modeling. This novel material provided potential applications to remove radionuclide from wastewater pollutants.

2. Experimental section

2.1. Materials

Eu_2O_3 (Purity, 99.99%) was used to prepare Eu(III) stock solutions (300 $mg \cdot L^{-1}$) via being dissolved by concentrated HNO_3, evaporated, and diluted by 0.003 $mol \cdot L^{-1}$ HNO_3 solution. The main components of HA (from Gansu province, China) were C, N, O, S and the percentages of these components are respectively 60%, 4.21%, 31% and 0.52%. The other reagents were analytical grade from Sinopharm, China and not purified before using.

* Corresponding author at: Institute of Plasma Physics, Chinese Academy of Sciences, P.O. Box 1126, Hefei 230031, P.R. China.
E-mail address: huang2yn@mail.uc.edu (Y. Huang).

http://dx.doi.org/10.1016/j.molliq.2016.07.067
0167-7322/

2.2. Synthesis of CNFs

CNFs were synthesized as the literature reported [16]. Te nanowire templates were firstly synthesized. Specifically, 1.0 g polyvinylpyrrolidone (PVP) was added in 35 mL ultrapure water at room temperature, followed by adding Na_2TeO_3 (95 mg), $N_2H_4{\cdot}H_2O$ (1.8 mL) and $NH_3{\cdot}H_2O$ (3.5 mL). The above mixture was transferred in a Teflon-lined stainless autoclave, and maintained at 180 °C for 6 h, then cooled to room temperature. The precipitation of the product was obtained by adding acetone (30 mL) into a 10 mL above prepared solution. By centrifugation and filtration, the obtained precipitate was dispersed in a glucose solution (80 mL, 64 $g{\cdot}L^{-1}$) in an autoclave. The mixture was kept on 160 °C for 28 h before cooling to room temperature. By immersing into a mixed solution (V_{HNO3}:V_{H2O}:V_{H2O2} = 2:3:5), Te templates can be removed. The desired brown suspension was left, then further washed by ultrapure water and ethanol.

2.3. Characterization of CNFs

The characterization of CNFs included scanning electron microscopy (SEM), Fourier transform infrared spectroscopy (FT-IR), X-ray photoelectron spectroscopy (XPS), and potentiometric acid-base titration. The SEM images were taken from FEI-JSM 6320F scanning electron microscope. The FT-IR spectra were obtained from a Nicolet 8700 FT-IR spectrometer. The XPS spectra were characterized by the thermo ESCALAB 250 electron spectrometer. The C 1s peak at 284.4 eV was used as a reference to correct surface charging effects. The XPSPEAK41 program was used to resolve the C 1s and O 1s spectra. The potentiometric acid-base titration was performed by DL50 Automatic Titrator. Specifically, CNFs (0.05 g) were spiked into a $NaClO_4$ electrolyte (0.01 $mol{\cdot}L^{-1}$) at 288 K under argon atmosphere. $HClO_4$ (0.01 $mol{\cdot}L^{-1}$) was used to adjust the initial pH value to be 3.0, followed by slow titration with NaOH (0.04959 $mol{\cdot}L^{-1}$) to pH 10.0.

2.4. Batch adsorption experiments

Batch technique was used to investigate Eu(III) adsorption on CNFs at 15 ± 1 °C under N_2 protection. A mixed solution of CNFs and $NaClO_4$ was pre-equilibrated for 24 h, followed by adding the desired Eu(III) solutions to initiate the adsorption process. Negligible amount (0–20 μL) of $HClO_4$ or NaOH solution (0.01 or 0.1 mol/L) were added to reach the desired pH values from 2.0 to 10.0 for pH effect investigation. The pH of the adsorption isotherm was adjusted to be 4.5 ± 0.1. After the mixtures were shaken for 24 h, the CNFs were separated from the liquid phase by centrifugation (15,000 rpm, 20 min).

The concentration of Eu(III) in supernatant was determined by a Packard 3100 TR/AB liquid scintillation analyzer. All of the experimental data were averages of triplicate analysis results and the relative errors were within ±2%. The adsorption percentage ($R\%$) and distribution coefficients (K_d) of Eu(III) on the CNFs could be expressed as Eqs. (1) and (2).

$$R\% = (C_0 - C_e)/C_0 \times 100\% \quad (1)$$

$$K_d = (C_0 - C_e)\, V/C_e\, m \quad (2)$$

3. Results and discussion

3.1. Characterization

CNF microscopic characterization and potentiometric acid-base titration were collected in Figs. 1 and 2. The SEM and TEM images (Fig. 1A) showed that the as-prepared CNFs presented as flexible nanofibers of ca. 100 nm in diameter without the formation of any carbon spheres [17]. The deconvolution of O 1s and C 1s XPS spectra peaks of CNFs were shown in Fig. 2A and B. Three oxygen-containing functional groups were observed from the high resolved O 1s XPS spectrum (Fig. 2B), i.e., C—O at 533.5 eV, O—H at 532.5 eV, and C═O at 531.2 eV [18,19], indicating high oxidation degrees. From Fig. 2A, the high resolved C 1s spectrum can be divided into peaks of C—C, C—O—H, and C═O at 284.5, 285.2 and 287.7 eV, respectively [16,20]. FT-IR spectrum (Fig. 2C) further confirmed the existence of different oxygen containing functional groups, such as the O—H groups at 3438 cm^{-1}, C—O groups at 1290 cm^{-1} and 1213 cm^{-1}, and C═O groups at 1658 cm^{-1}, etc [21]. The acid-base titration data of the CNFs was presented in Fig. 2D, based on the reports [22,23]. It was shown that the point of zero charge (pH_{PZC}) of CNFs surface was about 3.96 from potentiometric acid-base titration (Fig. 2D). The surface charge of CNTs is positive at pH < pH_{PZC}, due to an excess of protons. At pH > pH_{PZC} the surface charge of CNTs is negative.

3.2. Effect of contact time

The effect of contact time on the Eu(III) adsorption efficiency on CNFs was presented in Fig. 3A. A fast initial adsorption was observed within the first 5 h, followed with a slow adsorption and reached the maximum value within 15 h. The fast adsorption within the first 5 h can be attributed to the rapid diffusion of Eu(III) from the solution to the active site of CNFs surfaces. It can be seen that slower increase in the adsorption curve at later stages, which may be caused by the longer diffusion range of Eu(III) into the pores of CNFs [24]. Chemical adsorption can be used to explain such fast adsorption of Eu(III) on CNFs surfaces [25]. The adsorption time will be set as 24 h to ensure the

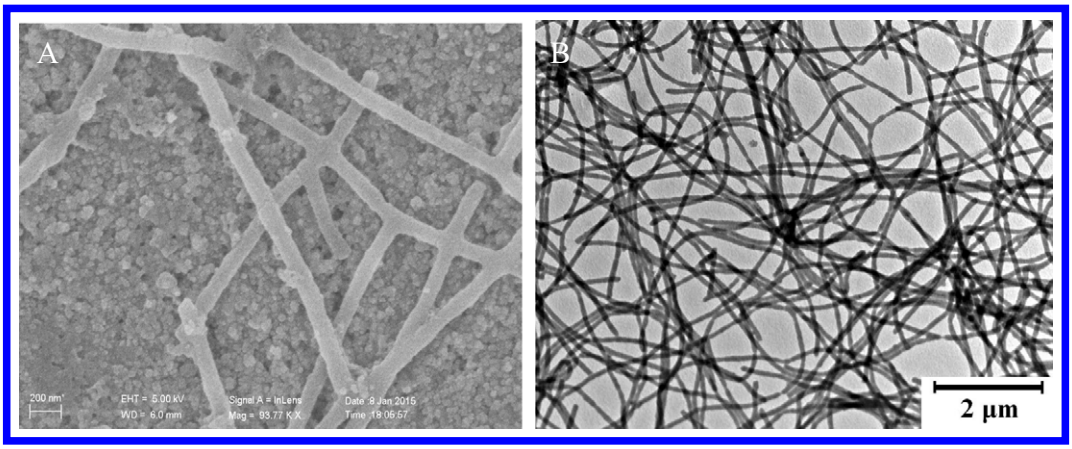

Fig. 1. Characterization of CNFs: (A) SEM image; (B) TEM image.

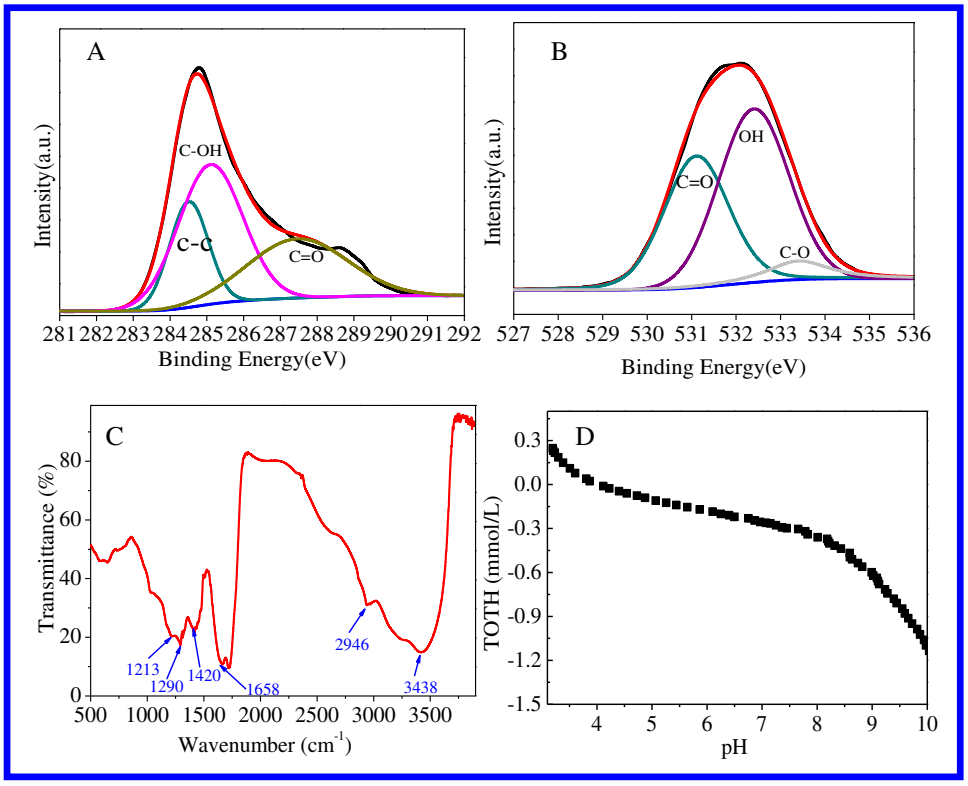

Fig. 2. (A) and (B): High resolved XPS spectra for C 1s and O 1s, respectively. The red and black line show overall spectra and test spectra; (C) FT-IR spectrum; (D) acid-base titration curve.

adsorption equilibrium in the following experiments. Two kinetic models are adopted to predict the characteristics and mechanisms of the Eu(III) adsorption on CNFs. The pseudo-first and pseudo-second order kinetic equations are presented as Eqs. (3) [26] and (4) [27], respectively:

$$\ln(q_e - q_t) = \ln q_e - k_f \cdot t \tag{3}$$

$$t/q_t = 1/k_s q_e^{\,2} + t/q_e \tag{4}$$

where q_t ($mg \cdot g^{-1}$) is the amount of Eu(III) adsorbed on CNFs at time t (h); q_e ($mg \cdot g^{-1}$) is the equilibrium adsorption capacity; k_f (h^{-1}) is the pseudo-first rate constant of adsorption, and k_s ($g \cdot (mg \cdot h)^{-1}$) is the pseudo-second-order rate constant of adsorption.

Table 1 collected the calculated parameters from both kinetic models, which indicated a preferred pseudo-second-order kinetic adsorption process over the pseudo-first-order kinetic model by comparing the correlation coefficients (R^2) of 0.997 and 0.880, respectively.

3.3. Effect of adsorbent concentration

The effect of adsorbent concentration on the Eu(III) adsorption on CNFs is given in Fig. 3C. The adsorption of Eu(III) on CNFs increased dramatically from 2.4–77.7% with increasing adsorbent concentration from 0.021–0.25 $g \cdot L^{-1}$. At a fixed initial Eu(III) concentration, more reactive sites on CNFs surfaces were available to combine with Eu(III) ions with increasing amount of CNFs, resulting in the increased adsorption efficiencies. The distribution coefficient (K_d) as a function of CNFs concentration was also presented in Fig. 3C. Slightly increased K_d values were observed with increasing adsorbent concentration under the experimental conditions. This trend is in consistent with the physicochemical properties of distribution coefficient, i.e., at very low adsorbent concentration, there is independence between the K_d values and the adsorbent concentration such as the adsorption of U(VI) on Na-attapulgite [28], the adsorption of U(VI) on iron oxyhydroxides [29]. The difference may be related with the characters of different adsorbents, the range of adsorbent concentration and the initial concentration of adsorbate.

3.4. Effect of pH and ionic strength

The effect of pH was carried out in a $NaClO_4$ solution (0.01 $mol \cdot L^{-1}$), as depicted in Fig. 3D. The adsorption increased quickly with the pH value ranging from 2.0 to 6.0, and the high adsorption percent was maintained at pH > 6.0. Based on the calculated solubility product constant of $Eu(OH)_3(s)$ ($K_{sp} = 3.4 \times 10^{-22}$) [30], the precipitation of $Eu(OH)_3(s)$ starts at pH = 8.2 and $C_{Eu3+} = 6.58 \times 10^{-5}$ mol/L. However, most Eu(III) ions (>90%) were observed to be adsorbed on CNFs at pH 6.0, indicating a minor factor of Eu(III) precipitation for the high efficient adsorption of Eu(III) on CNFs. The ionic strength effect was also investigated and carried out in different $NaClO_4$ solutions (0.001, 0.01 and 0.1 M) in Fig. 3D. An independent ionic strength effect was observed within the whole pH values. Based on the previous report that inner-sphere surface complexation was not sensitive to ionic strength variation as compared to outer-sphere surface complexation and cation exchange [31], the inner-sphere surface complexation is a dominant mechanism in the adsorption process. As observed from FTIR and XPS spectra, the presences of oxygen-containing functional groups on CNFs surfaces provided enough active sites for the complexation of CNFs surfaces with Eu(III), which were further corroborated by the surface complexation modeling studies.

3.5. Surface complexation modeling

The Visual MINTEQL software is used for fitting the adsorption of Eu(III) on CNFs surface [32–34]. The 2-pK model is selected to simulate the test data. 2-pK model is used to be one type of adsorbent's surface sites models, on which site both dissociation and protonation reactions can happen. ═SOH and ═XOH were used to represent the strong acidic

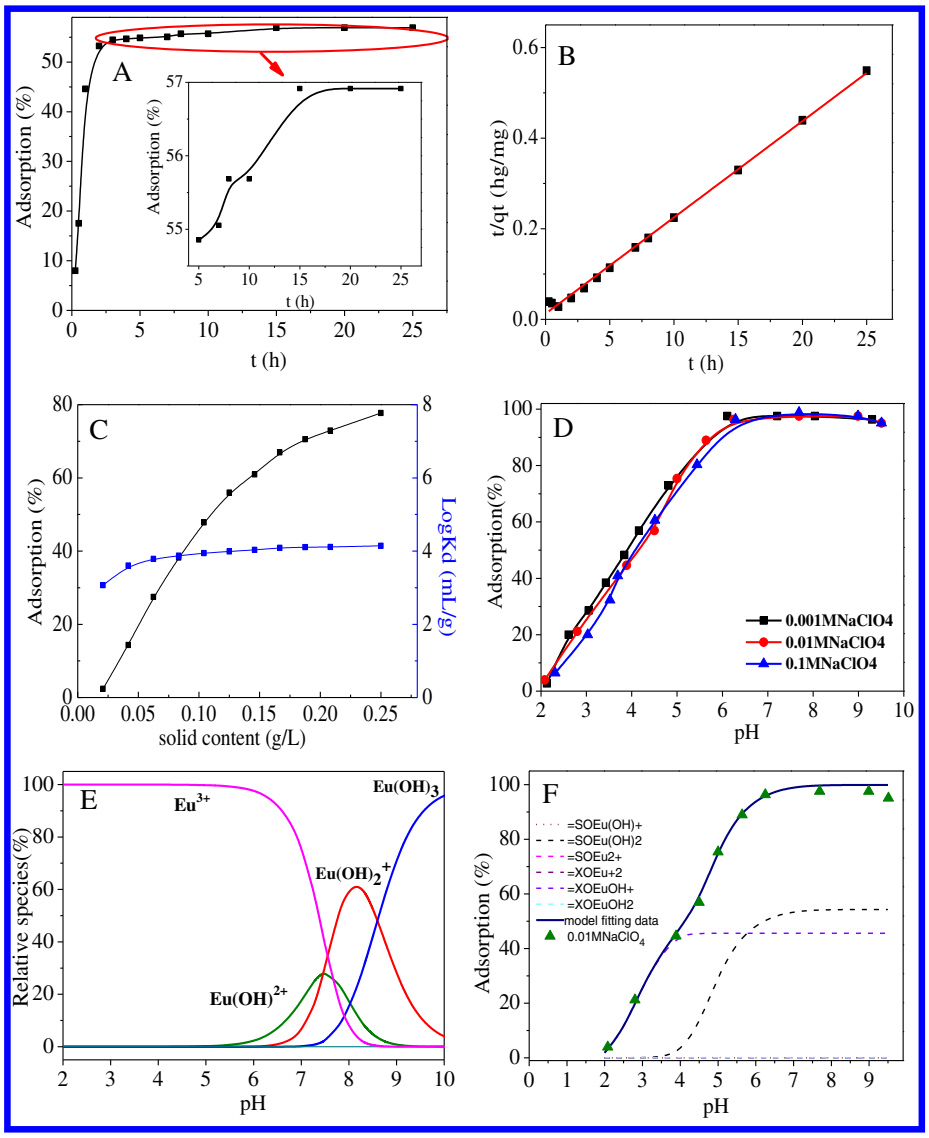

Fig. 3. (A): adsorption kinetics of Eu(III) on CNFs surfaces, $C_o = 10\ mg{\cdot}L^{-1}$, pH = 4.5, $I = 0.01\ mol{\cdot}L^{-1}\ NaClO_4$, m/V = 0.125 $g{\cdot}L^{-1}$, $T = 288$ K,(B): pseudo-second order kinetic model; (C): Effect of adsorbent content on Eu(III) adsorption onto CNFs. (D): Effect of pH on Eu(III) adsorption onto CNFs in presence of 0.01,0.1 and 1 mol/L $NaClO_4$ solutions. (E): Distribution of Eu(III) species as a function of pH, $C_o = 10\ mg{\cdot}L^{-1}$, $I = 0.01\ mol{\cdot}L^{-1}\ NaClO_4$, and $T = 288$ K. (F): Effect of pH, $C_o = 10\ mg{\cdot}L^{-1}$, m/V = 0.125 $g{\cdot}L^{-1}$, $I = 0.01\ mol{\cdot}L^{-1}\ NaClO_4$, $T =$ 288 K, the solid line and dash lines are model fitting curves and Eu(III) surface complexes respectively.

groups (carboxyl group) and the weak ones (hydroxyl group). Based on the Eu(III) distribution chart (Fig. 3E), Eu^{3+} is the main Eu(III) form at pH < 5.5, and three forms ($Eu(OH)^{2+}$, $Eu(OH)_2^+$ and $Eu(OH)_3$) coexist between 5.5 and 10.0. To simplify the adsorption process, at pH < 10, Eu^{3+}, $Eu(OH)^{2+}$ and $Eu(OH)_2^+$ species were used to optimize the adsorption data. The surface complexation reactions between Eu(III) and CNFs are presumed by Eqs. (5)–(13):

$$\equiv SOH + H^+ \rightarrow \equiv SOH_2^+ \quad (5)$$

Table 1
The calculated parameters of pseudo-first and pseudo-second order kinetic models.

Kinetic models	$q_e\ (mg{\cdot}g^{-1})$	$K_f\ (h^{-1})$	$K_s(g{\cdot}(mg\ h)^{-1})$	R^2
Pseudo-first order	19.1	0.438	–	0.880
Pseudo-second order	47.2	–	0.035	0.997

$$\equiv SOH \rightarrow \equiv SO^- + H^+ \quad (6)$$

$$\equiv XOH \rightarrow \equiv XO^- + H^+ \quad (7)$$

$$\equiv SOH + Eu^{3+} \rightarrow \equiv SOEu^{2+} + H^+ \quad (8)$$

$$\equiv SOH + Eu^{3+} + H_2O \rightarrow \equiv SOEu(OH)^+ + 2H^+ \quad (9)$$

$$\equiv SOH + Eu^{3+} + 2H_2O \rightarrow \equiv SOEu(OH)_2 + 3H^+ \quad (10)$$

$$\equiv XOH + Eu^{3+} \rightarrow \equiv XOEu^{2+} + H^+ \quad (11)$$

$$\equiv XOH + Eu^{3+} + H_2O \rightarrow \equiv XOEu(OH)^+ + 2H^+ \quad (12)$$

$$\equiv XOH + Eu^{3+} + 2H_2O \rightarrow \equiv XOEu(OH)_2 + 3H^+ \quad (13)$$

The values of logK of Eqs. (5)–(7) are achieved from the results fitting the potentiometric titration of CNFs. The log K values of Eqs.

Table 2
Surface complexation reactions of Eu(III) adsorption on CNFs.

Surface complexation reactions	Equilibrium adsorption constants (*logK*)
$\equiv SOH + H^+ \rightarrow \equiv SOH^{2+}$	−3.98
$\equiv SOH \rightarrow \equiv SO^- + H^+$	−5.0
$\equiv XOH \rightarrow \equiv XO^- + H^+$	−5.8
$\equiv SOH + Eu^{3+} \rightarrow \equiv SOEu^{2+} + H^+$	−5.4
$\equiv SOH + Eu^{3+} + H_2O \rightarrow \equiv SOEu(OH)^+ + 2H^+$	−0.65
$\equiv SOH + Eu^{3+} + 2H_2O \rightarrow \equiv SOEu(OH)_2 + 3H^+$	−4.8
$\equiv XOH + Eu^{3+} \rightarrow \equiv XOEu^{2+} + H^+$	−2.5
$\equiv XOH + Eu^{3+} + H_2O \rightarrow \equiv XOEu(OH)^+ + 2H^+$	−1.8
$\equiv XOH + Eu^{3+} + 2H_2O \rightarrow \equiv XOEu(OH)_2 + 3H^+$	−4.5

(8)–(13) are achieved by best fitting of the adsorption of Eu(III) on CNFs (Table 2). As compared with the experimental data, similar curves can be obtained over the studied pH ranges (Fig. 3F), indicating the sufficiency of the above adsorption reactions and the reliability of this model to the experimental adsorption data.

As seen from Fig. 3F, the predominate Eu(III) species on CNFs existed as $\equiv XOEu(OH)^+$ complex at pH < 3.5 and a mixture of $\equiv XOEu(OH)^+$ and $\equiv SOEu(OH)_2$ complexes at pH > 3.5, further confirming the dominant inner-sphere surface complexation.

3.6. Effect of humic acid (HA)

HA is a natural organic matter that was applied for the effect of natural organic matters towards the adsorption of many heavy metals [35,36]. The HA effect was also considered as a function of pH (Fig. 4A). Fig. 4A showed the effect of no HA and 10 mg·L^{-1} HA on the Eu(III) adsorption. The 10 mg·L^{-1} HA facilitated the adsorption kinetics of Eu(III) on the CNFs below pH 6.0, while decreased kinetics were observed at pH > 7.0. The electrostatic attraction forces were attributed for the high adsorption kinetics at low pH values. As a macromolecule, HA can also interact and form complexes with Eu(III) ions with lower formation energies and stronger complexation interactions than CNFs. Thus, the adsorbed HA on CNFs surfaces would also interact with Eu(III), resulting in an increased adsorption kinetics. However, the adsorbed HA on CNFs surfaces can be dissolved at higher pH values. In this case, HA and CNFs will competitively complex with Eu(III), resulting in lower adsorption kinetics.

Table 3
Parameters for the Langmuir and Freundlich Models of Eu(III) adsorption on CNFs.

	Langmuir model			Freundlich model		
T (K)	Q_{max} (mg·g^{-1})	K_L (L·mg^{-1})	R^2	k_F (mg^{1-n}·L^{n}g^{-1})	n	R^2
288	62.6	0.657	0.968	30.4	0.212	0.880
303	74.4	1.035	0.983	40.4	0.187	0.820
318	84.5	1.171	0.980	45.8	0.193	0.862

3.7. Adsorption isotherms and thermodynamic parameters

Fig. 4B shows the adsorption batch test results of Eu(III) on CNFs surfaces at 288, 303 and 318 K. Higher adsorption capacities are observed at higher temperatures. Both Langmuir and Freundlich models were applied to fit the experimental data. While the Langmuir model emphasized identical active sites on the surface of the adsorbent and a monolayer adsorption process [37], the Freundlich model focused on the heterogeneous solid surface with different binding energies [38]. The corresponding models are presented as Eqs. (14) and (15).

$$Q_e = Q_{max} \times K_L \times C_e/(1 + K_L C_e) \quad (14)$$

$$Q_e = K_F\, C_e^{\,n} \quad (15)$$

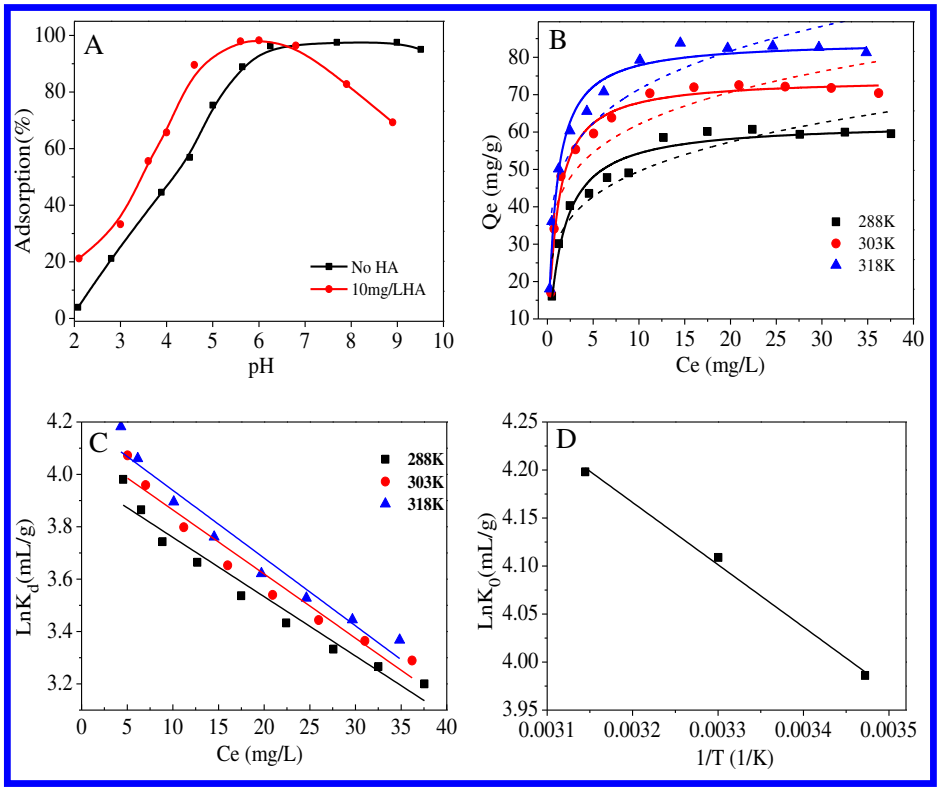

Fig. 4. (A) The effect of HA on Eu(III) adsorption onto CNFs, C_{HA} = 10 mg·L^{-1}, m/V = 0.125 g·L^{-1}, *I* = 0.01 mol·L^{-1} $NaClO_4$, *T* = 288 K. (B) adsorption isotherms at different temperatures, m/V = 0.125 g·L^{-1}, pH = 4.5, *I* = 0.01 mol·L^{-1} $NaClO_4$. The solid lines are the Langmuir model, and the dashed lines are the Freundlich model simulation.

Table 4
Comparison of maximum adsorption capacity of Eu(III) adsorption on various adsorbents.

Adsorbents	Experimental conditions	Adsorption capacity ($mg \cdot g^{-1}$)	Ref.
Bare TiO_2	pH = 4.5, T = 298 K	1.50	4
Na-montmorillonite	pH = 5.0, T = 298 K	1.02	6
MWCNTs	pH = 4.3, T = 298 K	7.33×10^{-6}	8
Activated carbon	pH = 4.5, T = 298 K	20.06	12
Graphene oxides	pH = 4.5, T = 298 K	161.08	12
CNFs	pH = 4.5, T = 288 K	62.6	This study

where Q_e ($mg \cdot g^{-1}$) is the adsorbed Eu(III), C_e ($mg \cdot L^{-1}$) is the equilibrated Eu(III) concentration. K_F ($(mg/g) \cdot (mg/L)^{-1/n}$) and K_L ($L \cdot mg^{-1}$) are the corresponding constants. Q_{max} ($mg \cdot g^{-1}$) is the theoretical saturation capacity. The value of n indicates the degree of adsorption capacity with equilibrium concentration in aqueous solutions. The simulated data of two models are collected in Table 3, which clearly indicated a better fitting line by the Langmuir model ($R^2 > 0.96$), indicating a dominant monolayer adsorption between Eu(III) and the CNFs. The Q_{max} calculated from the Langmuir model at 288, 303 and 318 K are 62.6, 74.4 and 84.5 $mg \cdot g^{-1}$, respectively, indicating promoted adsorption capacities at higher temperatures and an endothermic adsorption process. Various materials have been used as adsorbents to Eu(III), shown in Table 4. the values of Q_{max} of commercial titanium dioxide, Na-montmorillonite, MWCNTs, activated carbon, graphene oxide were 1.50, 1.02, 7.33×10^{-6}, 20.06 and 161.29 $mg \cdot g^{-1}$, respectively. The adsorption capacity of CNFs is higher than other materials except graphene oxide (GO). Due to high surface area and many oxygen-containing functional groups, there are high adsorption capacity of GO to heavy metal ion and radionuclides adsorption [39,40]. Meanwhile, due to the good hydrophilicity, GO is not easy to be separated from water phase. However, CNFs is a promising material in the construction of 2D macroscopic membranes for water filtration.

Thermodynamic parameters, including $\Delta H°$, $\Delta S°$, and $\Delta G°$ can be calculated from the adsorption isotherms at different temperatures with the aid of the following Eqs. (16) and (17).

$$\Delta G^\circ = RT \ln K_d = \Delta H^\circ - T\Delta S^\circ \quad (16)$$

$$\ln K^\circ = \Delta S^\circ / R - \Delta H^\circ / RT \quad (17)$$

where R (8.314 J mol^{-1} K^{-1}) is the universal gas constant and T (K) is temperature. By plotting $\ln K_d$ versus Ce, the adsorption equilibrium constant, K^0, can be calculated (Fig. 4C and D), while the values of ΔH^0 and ΔS^0 can be calculated by plotting $\ln K^0$ vs. $1/T$. The related thermodynamic data are collected in Table 5. Negative ΔG^0 values (-9.59 $kJ \cdot mol^{-1}$ at 288 K, -10.37 $kJ \cdot mol^{-1}$ at 303 K, and -11.15 $kJ \cdot mol^{-1}$ at 318 K) indicated a spontaneous process, and higher temperatures were more favorable as decreased values of ΔG^0 were observed with increasing temperatures. Positive value of $\Delta H°$ indicated an endothermic adsorption process, which can be attributed to the dehydration/recombination phenomenon. While the dehydration from hydrous Eu(III) is an endothermic process, the recombination of dehydrated Eu(III) on CNFs is an exothermic process. In this case, higher dehydration process exceeded the recombination process, resulted in an endothermic adsorption. Moreover, a slightly increased degree of randomness was observed from the calculated positive $\Delta S°$ value (0.052 $kJ \cdot (mol \cdot K)^{-1}$). Overall, the thermodynamic results revealed that the adsorption of Eu(III) on CNFs surfaces is a spontaneous and endothermic process.

Table 5
Thermodynamic parameters for Eu(III) adsorption on CNFs.

$\Delta H°$	$\Delta S°$	$\Delta G°$ ($kJ \cdot mol^{-1}$)		
($kJ \cdot mol^{-1}$)	($kJ \cdot mol^{-1} \cdot K^{-1}$)	T = 288 K	T = 303 K	T = 318 K
5.39	0.052	−9.59	−10.37	−11.15

4. Conclusions

In this paper, CNFs were successfully fabricated and characterized by microscopic techniques and potentiometric acid-base titration. The adsorption of Eu(III) on CNFs surfaces was influenced by pH values, but independent of ionic strengths. The interactions between Eu(III) and CNFs were simulated from surface complexation modeling and determined to form $\equiv XOEu(OH)^+$ and $\equiv SOEu(OH)_2$ complexes. This paper highlighted the potential applications of CNFs to remove radionuclides from wastewater pollutants.

Acknowledgments

Special scientific research fund of public welfare profession of China (201509074), National Natural Science Foundation of China (No. 41273134; 21477133; 91326202) are acknowledged.

References

[1] Y.B. Sun, C.C. Ding, W.C. Cheng, X.K.J. Wang, Hazard. Mater. 280 (2014) 399–408.
[2] X.L. Tan, X.K. Wang, H. Geckeis, T. Rabung, Environ. Sci. Technol. 42 (2008) 6532–6537.
[3] N. Janot, M.F. Benedetti, P.E. Reiller, Environ. Sci. Technol. 45 (2011) 3224–3230.
[4] X.L. Tan, M. Fang, J.X. Li, Y. Lu, X.K.J. Wang, Hazard. Mater. 168 (2009) 458–465.
[5] M. Bouby, J. Lutzenkirchen, K. Dardenne, T. Preocanin, M.A. Denecke, R. Klenze, H. Geckeis, J. Colloid Interface Sci. 350 (2010) 551–561.
[6] Y.B. Sun, J.X. Li, X.K. Wang, Geochim. Cosmochim. Acta 140 (2014) 621–643.
[7] Y.B. Sun, R. Zhang, C.C. Ding, X.X. Wang, W.C. Cheng, C.L. Chen, X.K. Wang, Geochim. Cosmochim. Acta 180 (2016) 51–65.
[8] Q.H. Fan, D.D. Shao, J. Hu, C.L. Chen, W.S. Wu, X.K. Wang, Radiochim. Acta 97 (2009) 141–148.
[9] G. Accorsi, N. Armaroli, A. Parisini, M. Meneghetti, R. Marega, M. Prato, D. Bonifazi, Adv. Funct. Mater. 17 (2007) 2975–2982.
[10] C.L. Chen, X.K. Wang, M. Nagatsu, Environ. Sci. Technol. 43 (2009) 2362–2367.
[11] Y.B. Sun, Q. Wang, C.L. Chen, X.L. Tan, X.K. Wang, Environ. Sci. Technol. 46 (2012) 6020–6027.
[12] Y.B. Sun, D.D. Shao, C.L. Chen, S.B. Yang, X.K. Wang, Environ. Sci. Technol. 47 (2013) 9904–9910.
[13] B. Hu, K. Wang, L. Wu, S.H. Yu, M. Antonietti, M.M. Titirici, Adv. Mater. 22 (2010) 813–828.
[14] H.W. Liang, X. Cao, W.J. Zhang, H.T. Lin, F. Zhou, L.F. Chen, S.H. Yu, Adv. Funct. Mater. 21 (2011) 3851–3858.
[15] Y.J. Zhong, S.J. You, X.H. Wang, X. Zhou, Y. Gan, N.Q. Ren, Chem. Eng. J. 226 (2013) 217–226.
[16] R. Zhang, C.L. Chen, J. Li, X.K. Wang, J. Colloid Interface Sci. 460 (2015) 237–246.
[17] C.C. Ding, W.C. Cheng, Y.B. Sun, X.K. Wang, Geochim. Cosmochim. Acta 165 (2015) 86–107.
[18] Y.B. Sun, S.B. Yang, C.C. Ding, W.C. Cheng, Z.X. Jin, RSC Adv. 5 (2015) 24886–24892.
[19] Z.X. Jin, X.X. Wang, Y.B. Sun, Y.J. Ai, X.K. Wang, Environ. Sci. Technol. 49 (2015) 9168–9175.
[20] W.C. Cheng, C.C. Ding, X.X. Wang, Z.Y. Wu, Y.B. Sun, S.H. Yu, T. Hayat, X.K. Wang, Chem. Eng. J. 293 (2016) 311–318.
[21] Y.B. Sun, Z.Y. Wu, X.X. Wang, C.C. Ding, W.C. Cheng, S.H. Yu, X.K. Wang, Environ. Sci. Technol. 50 (2016) 4459–4467.
[22] C.L. Chen, J. Hu, D. Xu, X.L. Tan, Y.D. Meng, X.K. Wang, J. Colloid Interface Sci. 323 (2008) 33–41.
[23] Y.B. Sun, C.L. Chen, X.L. Tan, D.D. Shao, J.X. Li, G.X. Zhao, S.B. Yang, Q. Wang, X.K. Wang, Dalton Trans. 41 (2012) 13388–13394.
[24] C.C. Ding, W.C. Cheng, Y.B. Sun, X.K.J. Wang, Hazard. Mater. 295 (2015) 127–137.
[25] Y.B. Sun, C.L. Chen, D.D. Shao, J.X. Li, X.L. Tan, G.X. Zhao, S.B. Yang, X.K. Wang, RSC Adv. 2 (2012) 10359–10364.
[26] S. Lagergren, Kungl. Svenska Vetenskapsakad Handl. 24 (1898) 1–39.
[27] Y.S. Ho, G. McKay, Process Saf. Environ. Prot. 76 (1998) 183–191.
[28] W.C. Cheng, C.C. Ding, Y.B. Sun, X.K. Wang, Chem. Eng. J. 269 (2015) 1–8.
[29] Y.B. Sun, S.T. Yang, G.D. Sheng, Z.Q. Guo, X.K. Wang, Radiochim. Acta 100 (2012) 779–784.
[30] Q.H. Fan, X.L. Tan, J.X. Li, X.K. Wang, W.S. Wu, G. Montavon, Environ. Sci. Technol. 43 (2009) 5776–5782.
[31] Y.B. Sun, S.B. Yang, Y. Chen, C.C. Ding, W.C. Cheng, X.K. Wang, Environ. Sci. Technol. 49 (2015) 4255–4262.
[32] J. Buffle, H.P. van Leeuwen, In Situ Monitoring of Aquatic Systems. Chemical Analysis and Speciation, in: J. Buffle, G. Horvai (Eds.), IUPAC Series on Analytical and Physical Chemistry of Environmental Systems, Vol. 6, John Wiley and Sons, Chichester 2000, p. 623.
[33] C.C. Ding, W.C. Cheng, Y.B. Sun, X.K. Wang, Dalton Trans. 43 (2014) 3888–3896.

[34] J.Y. Huang, Z.W. Wu, L.W. Chen, Y.B. Sun, J. Mol. Liq. 209 (2015) 753–758.
[35] Y.B. Sun, S.B. Yang, G.X. Zhao, Q. Wang, X.K. Wang, Chem. Asian. J. 8 (2013) 2755–2761.
[36] Z.X. Jin, H.Y. Gao, L.H. Hu, RSC Adv. 5 (2015) 88520–88528.
[37] I.J. Langmuir, Am. Chem. Soc. 40 (1918) 1361–1403.
[38] H. Freundlich, Z. Phys. Chem.–Stoch. Ve. 57 (1906) 385–470.
[39] S.J. Yu, X.X. Wang, X.L. Tan, X.K. Wang, Inorg. Chem. Front. 2 (2015) 593–612.
[40] X.X. Wang, S.B. Yang, W. Shi, J.X. Li, T. Hayat, X.K. Wang, Environ. Sci. Technol. 49 (2015) 11721–11728.